Numerical simulation of condensation of supercritical water gasification products in a supersonic nozzle

International Journal of Fluid Engineering 国际流体工程(英文)

RESEARCH ARTICLE | OCTOBER 10 2024

Numerical simulation of condensation of supercritical water gasification products in a supersonic nozzle

Hongtu Wu ; Mišo Jurčević; Henrik Ström ; Muhammad Shahzad Khurram ; Hui Jin

International Journal of Fluid Engineering 1, 043903 (2024)
https://doi.org/10.1063/5.0223253

International Journal of Fluid Engineering

RESEARCH ARTICLE

pubs.aip.org/hgmri/ijfe

Editor's Pick

Numerical simulation of condensation of supercritical water gasification products in a supersonic nozzle

Cite as: Int. J. Fluid Eng. 1, 043903 (2024); doi: 10.1063/5.0223253
Submitted: 13 June 2024 • Accepted: 18 September 2024 •
Published Online: 10 October 2024

Hongtu Wu,[1] Mišo Jurčević,[2] Henrik Ström,[3] Muhammad Shahzad Khurram,[4] and Hui Jin[1,a)]

AFFILIATIONS

[1] State Key Laboratory of Multiphase Flow in Power Engineering (SKLMF), Xi'an Jiaotong University, 28 Xianning West Road, Xi'an 710049, Shaanxi, China
[2] LTEF—Laboratory for Thermodynamics and Energy Efficiency, Faculty of Electrical Engineering, Mechanical Engineering and Naval Architecture (FESB), University of Split, Rudjera Boskovica 32, 21000 Split, Croatia
[3] Chalmers University of Technology, Göteborg, Sweden
[4] COMSATS, Lahore, Pakistan

[a)] **Author to whom correspondence should be addressed:** jinhui@mail.xjtu.edu.cn, **Tel.:** +86 029 82660876

ABSTRACT

The clean and efficient separation of supercritical water gasification products (SCWGP) has emerged as a significant challenge in supercritical water gasification technology. This paper proposes the use of a supersonic nozzle for the condensation and separation of H_2 and CO_2 from SCWGP, leveraging the high-pressure characteristics of these products. By establishing a flow model and a condensation model for the supersonic nozzle, the effects of inlet pressure and inlet temperature on the condensation process are analyzed. The analysis reveals that the latent heat released during condensation causes an abnormal distribution of pressure and temperature within the nozzle. When the inlet pressure of the nozzle is increased from 7.0 to 9.0 MPa, the liquid phase mass fraction at the outlet rises from 5.3×10^{-3} to 0.056. Similarly, when the inlet temperature is lowered from 300.0 to 290.0 K, the liquid phase mass fraction at the outlet also rises from 5.3×10^{-3} to 0.058. The increase in inlet pressure leads to the condensation location shifting toward the throat by $\sim 8.5 \times 10^{-3}$ m·MPa^{-1}, while the impact of inlet temperature is approximately -2.3×10^{-3} m·K^{-1}. The nucleation rate in the nozzle is always concentrated in a small region.

NOMENCLATURE

a_0	molecular surface area (m^2)
c	local velocity of sound (m·s^{-1})
dr/dt	droplet growth rate (m·s^{-1})
E	total energy (J)
h_{fg}	latent heat of vaporization (J)
h_t	total enthalpy (J)
J	condensation rate (m^{-3}·s^{-1})
Kn	Knudsen number
k_B	Boltzmann constant (J·K^{-1})
k_{eff}	effective thermal conductivity (W·m^{-1}·K^{-1})
L	length of converging section (m)
l	molecular mean free range (m)
Ma	Mach number
N	number of small droplets
Pr_g	Prandtl number
p_c	critical pressure (Pa)
p_g	gas pressure (Pa)
p_s	saturation pressure (K)
R_g	gas constant (J·kg^{-1}·K^{-1})
r	radius of small droplets (m)
r_c	critical size of condensation nucleus (m)
r_{in}	radius of nozzle inlet (m)
r_n	radius of nozzle at x (m)
r_t	radius of nozzle throat (m)
S	supersaturation degree
T_b	boiling temperature (K)

T_c critical temperature (K)
T_r contrast temperature (K)
T_s saturation temperature (K)
u velocity ($m \cdot s^{-1}$)
Y mass fraction of liquid phase

Greek

Γ rate of liquid phase formation ($kg \cdot m^{-3} \cdot s^{-1}$)
γ specific heat ratio
ε empirical constant
ρ_l density of liquid phase ($kg \cdot m^{-3}$)
σ surface tension ($N \cdot m^{-1}$)
τ_{eff} effective stress tensor (Pa)

I. INTRODUCTION

Over the past decade, the global demand for energy consumption has seen a steady and significant increase. This surge can be primarily attributed to two major factors: rapid population growth and ongoing industrial development across various regions. As more people inhabit the planet and industries continue to expand, the need for energy to power homes, businesses, and technological advances has escalated, placing additional pressure on global energy resources. Despite ongoing efforts to increase the share of renewable energy in the global energy mix, fossil fuels continue to hold a dominant position in the market. This highlights the challenge of transitioning to cleaner energy sources, as traditional fossil fuels remain the primary energy supply despite significant advances and investment in renewable energy technologies.[1] This dominance persists even as governments and organizations worldwide push for a transition toward more sustainable energy sources.[2]

The increased use of fossil fuels[3] has caused carbon dioxide levels in the atmosphere to skyrocket,[4] leading to an urgent need to find new energy consumption models that are low-carbon or even zero-carbon.[5] Amid the current energy landscape, where there is a growing emphasis on reducing carbon emissions, hydrogen has emerged as the primary choice for a carbon-neutral energy carrier.[6] Its potential to provide a sustainable and clean alternative to fossil fuels positions hydrogen as a key component in the global effort to achieve carbon neutrality and address the challenges of climate change.[7] Traditional methods of hydrogen production primarily involve techniques such as steam reforming, partial oxidation, and pyrolysis. These processes typically utilize a variety of sources, including fossil fuels like coal and methane. Another method is the production of hydrogen through electrolysis of water, but owing to its high energy demand, only a small portion of global hydrogen production is carried out using this method.[8] Owing to their renewability, materials and biomass by-products are considered to have great potential for hydrogen production.[8] Supercritical water gasification (SCWG) has emerged as a promising technology for clean hydrogen production. This innovative method is particularly effective in the utilization and conversion of solid waste and biomass, offering a sustainable approach to generating hydrogen.[9] By leveraging SCWG, industries can efficiently transform organic materials into hydrogen, contributing to a cleaner energy landscape and reducing reliance on fossil fuels.[10]

SCWG technology refers to the process in which biomass and other complex organic materials are decomposed into H_2, CO_2, and other by-products in a high-temperature, high-pressure water environment.[11] There has recently been growing research interest in SCWG, reflecting its potential as a cutting-edge solution for clean hydrogen production, with numerous investigations focusing on optimizing its processes and expanding its applications. These studies are crucial in advancing the technology and paving the way for its broader adoption in sustainable energy production.[12–14] However, little research has been done on the high-pressure mixed gas produced by SCWG, also known as SCWG products (SCWGP), which consists mainly of H_2 and CO_2. There is an urgent need to develop clean and efficient technologies for the separation and purification of SCWGP. Success in this will significantly promote the advancement and adoption of SCWG technology.

There have already been a number of studies of the separation of H_2 and CO_2 mixed gases. Abid *et al.*[15] investigated the effects on H_2/CO_2 separation of the modification of coal with CaO nanoparticles, while Shan *et al.*[16] explored the microstructure and separation mechanism of benzimidazole-linked polymer membranes (BLPMs) for the separation of H_2 and CO_2. Misawa *et al.*[17] developed an experimental system for the continuous separation of H_2 and CO_2 based on hydrate formation, using cyclopentane as a guest molecule. However, these separation methods have limitations, such as the inability to fully utilize the high-pressure energy inherent in SCWGP, and they rely on porous media and other chemicals for gas separation. Therefore, cleaner and more efficient separation technologies need to be developed specifically for SCWGP.

Supersonic nozzles are widely utilized in the separation and purification of CO_2-containing mixed gases, owing to their simple structure and high decarbonization efficiency. These nozzles effectively streamline the process of isolating and removing CO_2 from gas mixtures, making them a valuable tool in various industrial applications where reducing carbon emissions is a priority. Their efficiency and ease of use have made supersonic nozzles a preferred choice in technologies focused on gas purification and environmental sustainability. In supersonic nozzles, the expansion cooling effect causes CO_2 to undergo a phase change and form droplets during the flow process, thereby achieving CO_2 separation and purification.[18] Supersonic nozzles have already been applied to the separation of various mixed gases. The condensation processes within supersonic nozzles have been studied under a variety of conditions. For instance, Yin *et al.*[19] investigated the condensation of water vapor under varying backpressure conditions in a supersonic nozzle. Chen *et al.*[20] examined the condensation behavior of CO_2 within such a system. Sun *et al.*[21] performed computational fluid dynamics (CFD) simulations of the separation of H_2S/CH_4 mixed gases via condensation. Also adopting a numerical simulation approach, Sun *et al.*[22] applied different droplet growth models to investigate condensation processes of N_2, and Chen and Huang[23] modeled the condensation process of CO_2/N_2 mixed gases within a supersonic nozzle.

In the case of the high-pressure H_2/CO_2 mixed gases produced by SCWG, utilizing their pressure energy as they pass through a supersonic nozzle is one of the most optimal methods for achieving clean and efficient separation. Additionally, the use of a supersonic nozzle for separation is more easily integrated with the SCWG hydrogen production system, allowing for continuous and stable

production of higher-purity hydrogen in industrial settings. In the present study, the condensation process of SCWGP within a supersonic nozzle is modeled and analyzed. The distributions of relevant flow and condensation parameters inside the supersonic nozzle are determined and discussed, demonstrating the feasibility of condensing SCWGP within such a system. This study highlights the potential of using supersonic nozzles for effective condensation processes, paving the way for their innovative applications in hydrogen production and gas purification. Moreover, a series of key conclusions related to this condensation process are derived. Figure 1 provides a schematic of the process flow for condensing SCWGP using a supersonic nozzle, coupled with an SCWG system.

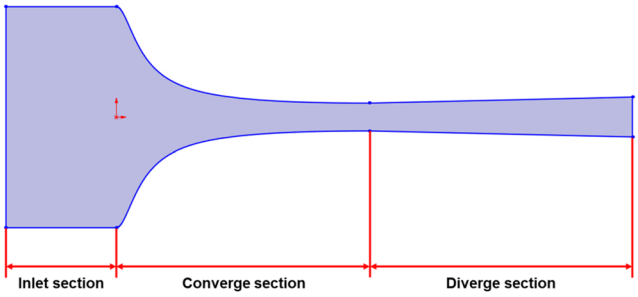

FIG. 2. Geometry of nozzle.

II. METHOD

A. Geometric model

Since the focus of this study is on the condensation of SCWGP within the device, and the process of droplets exiting the device outlet is not considered, only the most critical part of the condensation device—the supersonic nozzle—is taken into account.

During the condensation process of SCWGP, the mix enters the nozzle through its inlet. As the mixed gas flows through the system, the expansion effect of the nozzle causes the temperature of the gas to continuously decrease. This cooling effect is a direct result of the nozzle's ability to expand the gas, reducing its temperature throughout its passage through the system. This cooling effect eventually causes the gas mixture to reach its condensation temperature, leading to condensation of the components within the mixture. The liquefaction and separation of the mixed gases typically occur in the divergent section of the nozzle. This process is driven by the expansion of the mixed gases as they move through the divergent section, which causes their temperature to drop to the condensation temperature corresponding to the prevailing pressure. As a result, the gases condense and separate, making this section of the nozzle critical for effective gas liquefaction and separation in various industrial applications. The typical composition of SCWGP is a mixture of CO_2 and H_2. Owing to the significant differences in the properties of CO_2 and H_2, the CO_2 component of the mixture is more likely to liquefy into droplets during the condensation process. As a result, the droplets formed consist predominantly of CO_2, while the H_2-rich component remains in the gas phase. This process enables low-cost, efficient, and clean separation of SCWGP.

To study the separation of SCWGP, the nozzle model is simplified. The geometric model of the nozzle used for flow field calculations is shown in Fig. 2. The converging section of the nozzle is designed using the Witoszynski curve. Studies have demonstrated that nozzles designed using this specific method not only deliver excellent liquefaction performance, but are also remarkably easy to manufacture. Additionally, this design facilitates scaling up for mass production, making it highly suitable for large-scale industrial applications where efficient gas liquefaction and separation are required.[24] The mathematical expression for the Witoszynski curve is as follows:

$$r = \frac{r_t}{\sqrt{1 - \left[1 - \left(\frac{r_t}{r_{\text{in}}}\right)^2\right] \frac{\left(1 - \frac{x^2}{L^2}\right)^2}{\left(1 + \frac{x^2}{3L^2}\right)^3}}}, \tag{1}$$

where r is the radius of the nozzle at position x, r_t is the radius of the nozzle throat, r_{in} is the radius at the nozzle inlet, and L is the length of the converging section. Other important dimensional parameters of the nozzle used in the flow field simulation are presented in Table I.

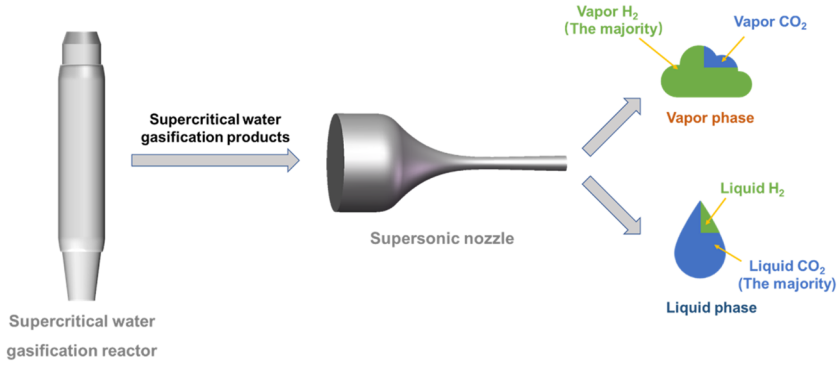

FIG. 1. Supersonic nozzle condensation separation system coupled with SCWG reactor.

TABLE I. Geometric parameters of nozzle.

Inlet length	40 mm
Inlet diameter	80 mm
Convergence length	91.8 mm
Throat diameter	10.08 mm
Divergence length	95.2 mm
Outlet diameter	14.45 mm

B. Phase transition model

The Navier–Stokes equations, combined with a phase change model that accounts for nucleation and droplet growth, are used to predict the complex condensation process. In this process, vortices coexist with supersonic flow, creating a dynamic environment where the interaction between these phenomena significantly influences the overall condensation behavior. This modeling approach is essential for accurately capturing the intricacies of phase transitions in high-speed flows, which is crucial for the design and optimization of advanced supersonic nozzles and related technologies. This model has been extensively studied and has been demonstrated to be applicable for simulating condensation in supersonic nozzles with various working fluids.[25,26] Since the droplet size is typically less than 1 μm, slip between the gas and liquid phases is neglected during the flow field simulation modeling procedure.[27] In the supersonic nozzle, where phase change occurs, the fluid entering the nozzle is in a gaseous state. Owing to the cooling effect of the nozzle, the fluid undergoes a phase change as it passes through, resulting in a gas–liquid mixture, rather than remaining in a single phase. This cooling effect also causes the CO_2 gas within the SCWGP to condense into a liquid as it flows through the nozzle, significantly impacting the flow dynamics and phase composition. Owing to the occurrence of this condensation process, it is necessary to take account of the changes in energy and mass in the gas phase due to the gas–liquid phase change. Additional source terms must be added to the flow governing equations. This modification is necessary to accurately account for the various physical processes and interactions that occur within the flow, ensuring that the equations reflect the full complexity of the system. The modified gas governing equations are as follows:[28]

$$\frac{\partial(\rho_g u_j)}{\partial x_j} + \frac{\partial \rho_g}{\partial t} = S_m, \tag{2}$$

$$\frac{\partial(\rho_g u_j u_i)}{\partial x_j} + \frac{\partial(\rho_g u_i)}{\partial t} + \frac{\partial p_g}{\partial x_i} + \frac{\partial(\rho_g \overline{u_i' u_j'})}{\partial x_j} = \frac{\partial}{\partial x_j}\left[\mu\left(\frac{\partial u_j}{\partial x_i} + \frac{\partial u_i}{\partial x_j} - \frac{2}{3}\delta\frac{\partial u_j}{\partial x_j}\right)\right] + S_u, \tag{3}$$

$$\frac{\partial}{\partial x_j}(\rho_g u_j E + u_j p_g) + \frac{\partial(\rho_g E)}{\partial t} = \frac{\partial}{\partial x_j}\left(k_{eff}\frac{\partial T}{\partial x_j} + u_i \tau_{eff}\right) + S_e, \tag{4}$$

$$S_m = -\Gamma, \tag{5}$$

$$S_u = -\Gamma u, \tag{6}$$

$$S_e = \Gamma(h_{fg} - h_t). \tag{7}$$

The governing equations for small droplets, which are derived from the results of previous studies, need to be established under certain assumptions. These assumptions are necessary to simplify the complex interactions and behaviors of the droplets, ensuring that the equations accurately represent the dynamics of the system while remaining feasible for practical use in further studies or applications.[29] To simplify the establishment and description of the liquid phase governing equations for a large number of small droplets, several assumptions are made: (1) it is assumed that the droplets and the gas have the same velocity, meaning that no velocity slip is considered; (2) the effects of gravity on the droplets are neglected; (3) the liquid phase is treated as a continuous medium; and (4) the droplets are assumed to be ideal spheres. These assumptions facilitate a more straightforward modeling approach by reducing the complexity of the system. Under these assumptions, the governing equations for the liquid phase in the supersonic nozzle can be expressed as follows:[30]

$$\frac{\partial}{\partial t}(\rho Y) + \frac{\partial}{\partial x_j}(\rho u_j Y) = S_Y, \tag{8}$$

$$\frac{\partial}{\partial t}(\rho N) + \frac{\partial}{\partial x_j}(\rho u_j N) = J, \tag{9}$$

$$r = \left(\frac{3}{4\pi}\frac{Y}{\rho_l N}\right)^{1/3}, \tag{10}$$

$$S_Y = \Gamma. \tag{11}$$

After the governing equations for both the gas and liquid phases have been established, the next essential task is to develop a condensation model. This model is crucial for accurately describing the gas–liquid phase transition, ensuring that the dynamics of this process are effectively captured and represented in the analysis. The model assumes that the gas involved in the process is either pure or contains only low levels of impurities, which allows for spontaneous condensation to occur. In such scenarios, nucleation, i.e., the spontaneous formation of condensation nuclei, plays a crucial role, because it marks the onset of the condensation process. However, studying nucleation is particularly challenging owing to its vigorous and complex nature at the microscopic scale. Various theories have been proposed to explain this phenomenon, many of which have been derived from classical nucleation theory, offering different perspectives on the initiation and development of condensation under various conditions. This paper adopts the condensation nucleation model proposed by Lamanna,[31] which has been recognized in previous investigations for its high accuracy in predicting nucleation processes and nucleation rates in high-speed flows (see, e.g., Ref. 32). The condensation model equations are as follows:[31]

$$J = \frac{\varepsilon}{S}\frac{\rho_g^2}{\rho_l}\exp\left[-\frac{16}{3}\frac{\pi\sigma^3}{k_B\rho_l^2 R_g^2 T^3(\ln S)^2}\right]\exp\left(\frac{\sigma a_0}{k_B T}\right)\sqrt{\frac{2\sigma}{\pi m_0^3}}, \tag{12}$$

$$S = \frac{p_g}{p_s}. \tag{13}$$

The growth of a large number of small droplets typically signifies the conclusion of the nucleation process. During this stage, the appearance of condensation nuclei becomes crucial, because these nuclei serve as attachment points for the supersaturated gas molecules in a nonequilibrium state. The condensation nuclei provide essential attachment sites, which strongly support the initial formation and subsequent growth of droplets. This provision of attachment sites facilitates the continued development of these droplets, playing a crucial role in driving the progression of the condensation process. Droplet growth is a process of gas–liquid phase transition and therefore involves latent heat. In this energy-changing process, the system transitions from a gaseous state to one of gas–liquid coexistence. Gyarmathy[33] made a significant contribution to the field by proposing a classical droplet growth model based on interphase heat transfer. This model is versatile and can be applied to various flow conditions, making it a valuable tool for understanding and analyzing the behavior of droplets across different scenarios in fluid dynamics. It has been applied to the simulation of condensation in supersonic nozzles, and experiments have verified that the model effectively captures the details of droplet growth in supersonic flows.[34] The model is described by the following equations:[33]

$$\frac{dr}{dt} = \frac{\lambda_g (T_s - T)\left(1 - \frac{r_c}{r}\right)}{\rho_l h_{fg} r\left(1 + Kn \frac{\gamma}{\gamma+1} \frac{2\sqrt{8\pi}}{1.5 Pr_g}\right)}, \tag{14}$$

$$Kn = \frac{l}{2r}, \tag{15}$$

$$r_c = \frac{2\sigma}{\rho_l R_g T \ln S}. \tag{16}$$

The rate of liquid phase formation and the surface tension are given by[35]

$$\Gamma = \frac{4\pi r_c^2}{3} \rho_l J + 4\pi r^2 \rho_l N \frac{dr}{dt}, \tag{17}$$

$$\sigma = p_c^{2/3} T_c^{1/3} Q (1 - T_r^{11/9}), \tag{18}$$

respectively, where

$$Q = 0.1196\left[1 + T_{br} \frac{\ln (p_c/1.013)}{1 - T_{br}}\right] - 0.279, \tag{19}$$

$$T_{br} = \frac{T_b}{T_c}. \tag{20}$$

The fundamental defining equations for the Mach number are

$$c = \sqrt{\gamma R_g T}, \tag{21}$$

$$Ma = u/c. \tag{22}$$

C. Numerical method

Numerical simulations of the supersonic nozzle were conducted using Ansys Fluent software, with the gas flow controlled by the governing equations within Fluent. The additional source terms generated by condensation were incorporated into the governing equations with source term descriptions written in the C language. The liquid phase equations, nucleation-related equations, and others were also described in C and integrated into the flow simulation calculations. The condensation calculations written in C were implemented during each iteration through Fluent's UDF and UDS modules. A pressure-based solver was employed, with fluid density calculated using the Soave–Redlich–Kwong equation, and the turbulence characteristics were computed using the k–ε turbulence model. To achieve more accurate simulation results, a second-order upwind scheme was used for the calculations.

Since the supersonic nozzle is designed for SCWGP, which typically consist of a mixture of H_2 and CO_2, this study focuses on the condensation of this composition within the nozzle to derive some quantitative and qualitative conclusions. In this scenario, the effects of trace gases on the mixture are ignored. It is assumed that the SCWGP are composed solely of H_2 and CO_2, with a molar ratio of 8:2. This simplifies the analysis by focusing on the primary components of the SCWGP, ignoring the potential influence of any minor gases present.

D. Model validation

To validate the accuracy of the numerical simulations established in this study, experimental data on the condensation of CO_2 in a supersonic nozzle provided by Lettieri *et al.*[36] were used. In their experiment, Lettieri *et al.* arranged 13 pressure sensors along the direction of the airflow in the nozzle to monitor the pressure at the corresponding locations. Pressure was chosen as the monitoring parameter for the condensation process for three reasons. The pressure distribution within a supersonic nozzle provides crucial insights into the state of the gas flow, revealing whether it is uniform, turbulent, or experiencing variations due to different factors. Specifically, the pressure distribution can pinpoint the initial location of condensation, commonly referred to as the Wilson point, where the gas begins to condense into liquid droplets. Furthermore, by analyzing the pressure fluctuations that occur during the condensation process, we can obtain valuable information about the intensities of both mass and heat transfer. These fluctuations serve as indicators of how vigorously the gas is interacting with itself and its surroundings, shedding light on the complex dynamics of the condensation process in high-speed flows.[37]

The relative root mean square error (RRMSE) between the simulation results and the actual results can be calculated from the information in Fig. 3 as follows:

$$\mathrm{RRMSE} = \sqrt{\frac{1}{N}\sum_{i=1}^{N} (\text{observed} - \text{simulated})^2} = 0.05. \tag{23}$$

From the convective field simulation results and the calculation of the RRMSE, it can be concluded that condensation occurs in the CO_2 flow within the supersonic nozzle. This condensation leads to an abrupt change in the energy of the flow system, resulting in condensation shock waves and subsequent pressure fluctuations. Since

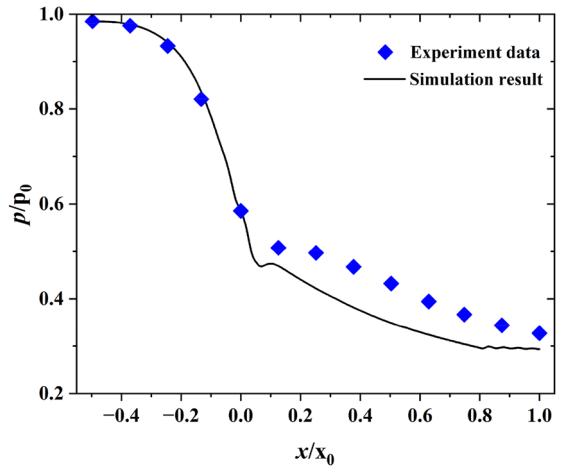

FIG. 3. Comparison of experimental data and simulation results for CO_2 condensation in a supersonic nozzle.

the condensation process of the fluid is inherently highly unstable, significant simplifications are often required when establishing a model to describe such a fluctuating process. This simplification can cause considerable deviations between simulation and the experiment. However, as shown in the validation results in Fig. 3, although there is some deviation between the simulation and the experiment after the condensation point, the overall RRMSE is not large. Moreover, the condensation flow simulation model that we have established effectively captures the pressure fluctuations caused by condensation. For the challenging simulation of nonequilibrium expansion condensation of high-speed gases in a supersonic nozzle, this deviation is considered acceptable. Therefore, the condensation model established in this study can be used to provide a series of quantitative and qualitative conclusions for the clean condensation separation of SCWGP.

Additionally, it is essential to perform a mesh analysis of the geometric model. Increasing the quality and density of the mesh can capture various critical parameters in the flow process more accurately. However, owing to computational limitations, the number of mesh elements cannot be increased indefinitely. On the basis of the

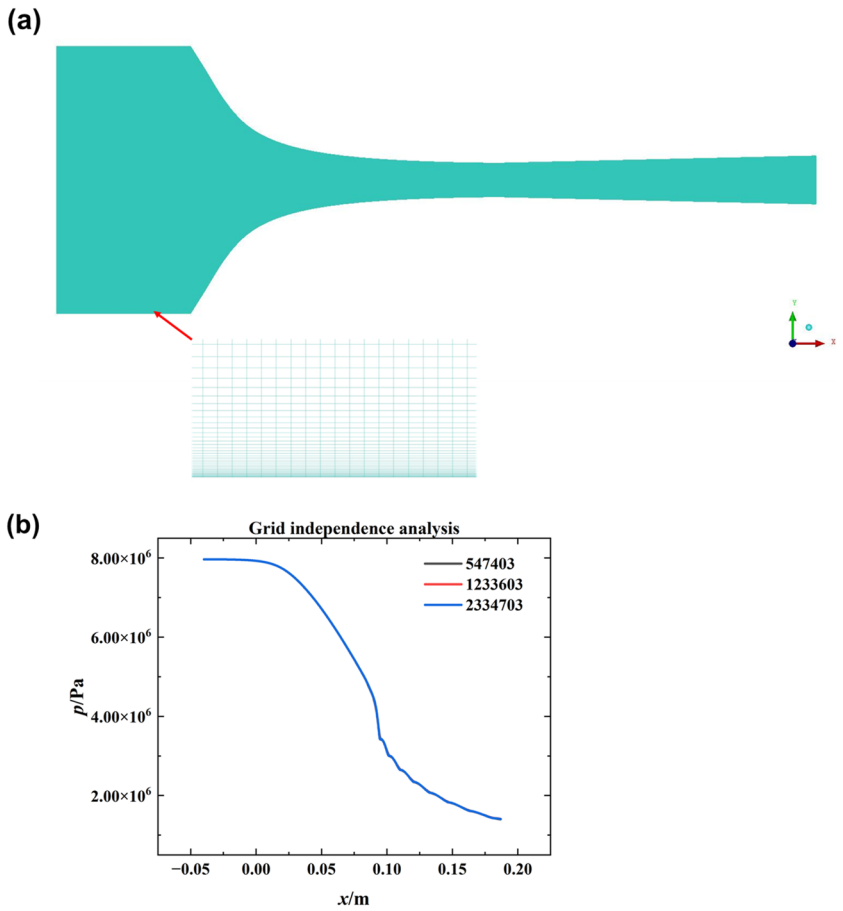

FIG. 4. Grid information for the supersonic nozzle: (a) grids for nozzle; (b) result of grid independence analysis.

above analysis, this study employs a structured mesh with a boundary layer mesh growth rate of 1.1 to refine the area near the nozzle wall. Figure 4(a) shows the mesh details, while Fig. 4(b) presents the variation in pressure distribution within the nozzle as the mesh count changes. From the computational results, it can be observed that at the nozzle outlet, when the mesh count increases from 547 403 to 1 233 603, the pressure calculation deviation is 0.49%, and when the mesh count increases from 1 233 603 to 2 334 703, it is 0.33%. This indicates that when the mesh count exceeds 547 403, the computational results tend to be accurate. Considering both computational speed and accuracy, the simulations in this study are all performed using a mesh with 1 233 603 elements.

III. RESULTS AND DISCUSSION

A. Influence of inlet pressure of supersonic nozzle on condensation process

From Fig. 5, it can be seen that when the inlet temperature is maintained at 300.0 K, both the pressure and temperature fields within the supersonic nozzle exhibit significant changes as the inlet pressure increases. The condensation process within the nozzle becomes more intense, indicating a stronger phase transition. Furthermore, the location at which condensation occurs shifts closer to the throat of the nozzle with increasing inlet pressure, highlighting the impact of pressure on the condensation of SCWGP.

The primary objective of this study is to quantitatively analyze the condensation process of SCWGP within a supersonic nozzle. To achieve this, it is necessary to take into account the symmetry of the nozzle, ensuring that the analysis accurately reflects the flow dynamics. The investigation focuses on key parameters along the centerline of the nozzle, including variations in pressure, temperature, liquid phase mass fraction, and Mach number. The study also explores how variations in inlet pressure can influence the specific location at which condensation occurs within the nozzle.

Figure 6 shows when the inlet temperature is held constant at 300.0 K, the pressure distribution along the nozzle centerline changes noticeably as the inlet pressure is increased from 7.0 to 9.0 MPa. However, it can also be seen that the variation in pressure at the nozzle outlet is significantly less than that at the inlet. Specifically, the outlet pressure shows a more modest increase, rising from 1.20 to 1.67 MPa. This indicates that with a 2.0 MPa increase in inlet pressure, the outlet pressure only increases by 0.47 MPa. This suggests that the supersonic nozzle can more effectively utilize the inlet pressure energy within the 7.0–9.0 MPa pressure range, allowing the SCWGP to fully expand and cool down within the nozzle. This is undoubtedly more beneficial for condensation within the nozzle. From the results for the pressure distribution along the nozzle centerline as the inlet pressure changes, it is clear that an appropriate increase in the inlet pressure will enable the supersonic nozzle to more fully utilize the pressure energy of the SCWGP, thereby achieving a cleaner and more energy-efficient separation.

Similarly, changes in the inlet pressure of the supersonic nozzle also cause significant variations in the temperature distribution along the nozzle centerline. Notably, owing to the condensation process of SCWGP within the nozzle, the temperature distribution exhibits a pattern different from the usual temperature profile in a nozzle. Generally, the temperature within a nozzle gradually decreases in the direction of fluid flow. However, the release of latent

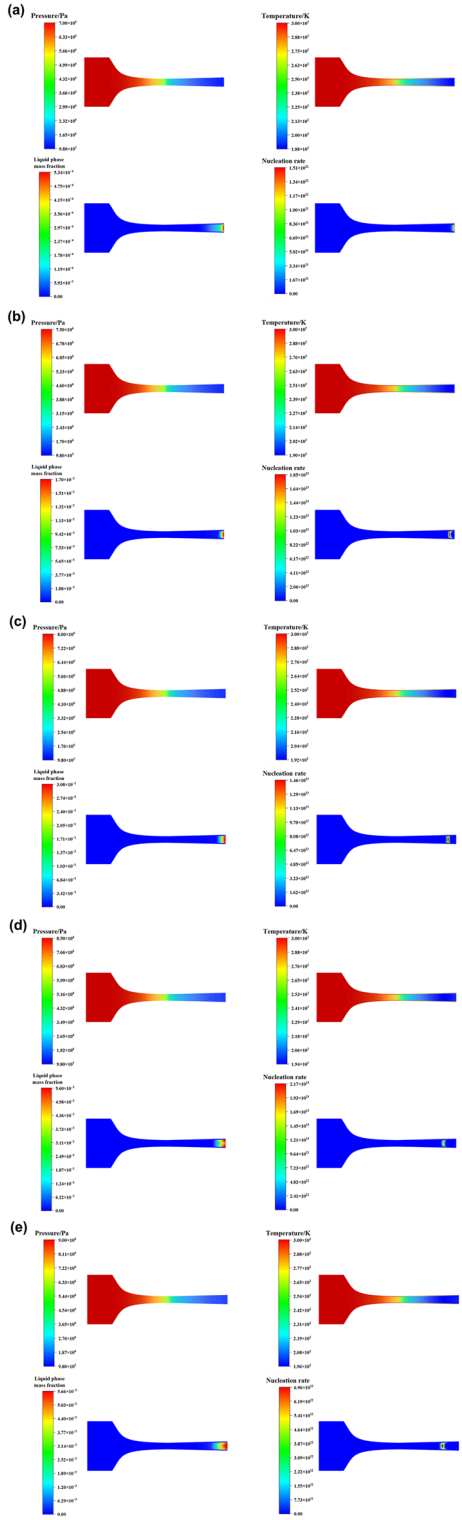

FIG. 5. Influence of the inlet pressure of a supersonic nozzle on the condensation process of SCWGP at an inlet temperature of 300.0 K: (a) 7.0 MPa; (b) 7.5 MPa; (c) 8.0 MPa; (d) 8.5 MPa; (e) 9.0 MPa.

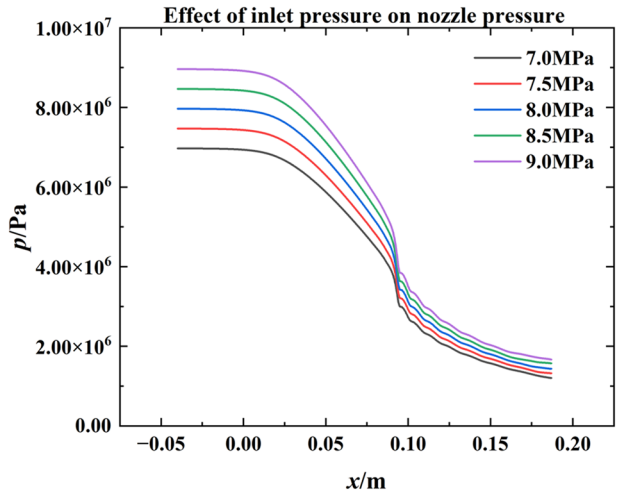

FIG. 6. Effect of inlet pressure on the centerline pressure distribution within the nozzle.

heat during condensation causes an abnormal increase in temperature at a certain point within the nozzle. When the inlet pressure of the nozzle increases from 7.0 to 9.0 MPa, the outlet temperature along the nozzle centerline rises from 188.0 to 200.6 K. As clearly shown in Fig. 7, as the inlet pressure increases, there is a corresponding rise in the outlet temperature within the supersonic nozzle. Additionally, the starting point of this temperature increase moves progressively closer to the throat of the nozzle with higher inlet pressure. This is because the increased inlet pressure intensifies condensation within the supersonic nozzle, causing the starting point of condensation for the SCWGP to move progressively toward the throat of the nozzle.

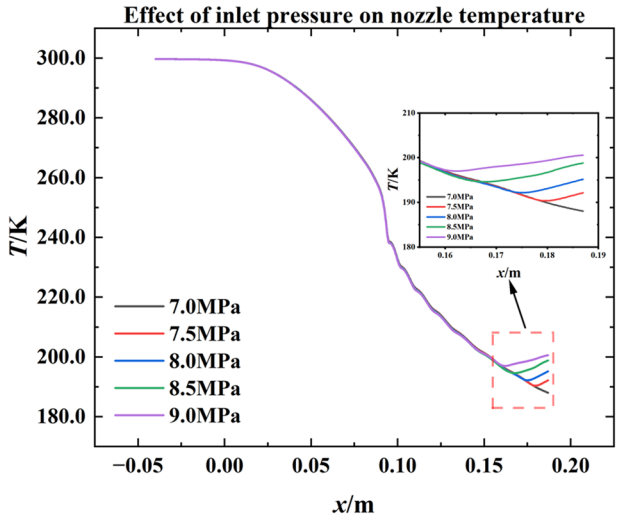

FIG. 7. Effect of inlet pressure on the centerline temperature distribution within the nozzle.

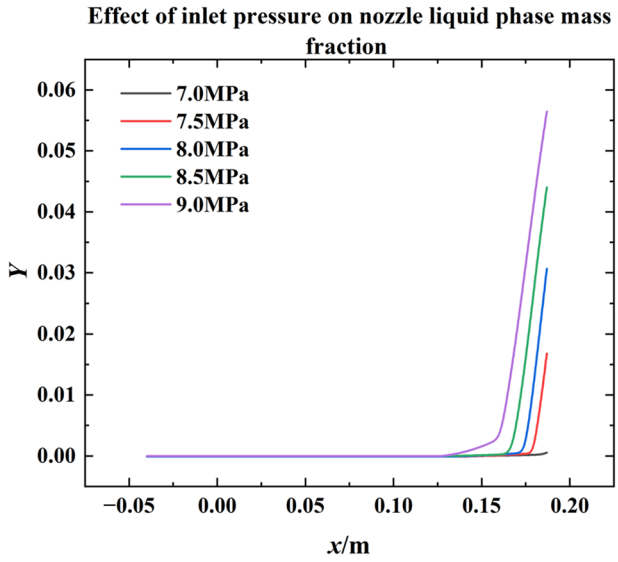

FIG. 8. Effect of inlet pressure on the centerline distribution of the liquid phase mass fraction within the nozzle.

Figure 8 shows the effect of inlet pressure variations on the liquid phase mass fraction along the centerline of the supersonic nozzle. When the inlet pressure is at 7.0 MPa, there is almost no significant increase in the liquid phase fraction within the nozzle, indicating that condensation is negligible at pressures below this threshold. However, as the inlet pressure increases, it has a pronounced effect on the condensation process, causing a sharp rise in the liquid phase fraction. Specifically, when the inlet pressure is increased from 7.0 to 9.0 MPa, the liquid phase mass fraction at the nozzle outlet rises substantially, from 5.3×10^{-4} to 0.056, demonstrating the strong influence of inlet pressure on the phase transition within the nozzle. At lower inlet pressures, a slight increase in pressure significantly enhances the condensation effect within the nozzle, indicating a transition from noncondensing to condensing conditions. As the inlet pressure increases, several noticeable effects are observed within the nozzle. One of the key changes is the shift in the onset of condensation; specifically, the starting point where the liquid phase mass fraction begins to rise moves closer to the throat of the nozzle. This shift suggests that higher inlet pressures push the condensation process upstream, bringing it nearer to the throat. Additionally, higher inlet pressures result in a greater liquid phase mass fraction at the same location within the flow.

Figure 9 illustrates the impact of inlet pressure on the Mach number distribution along the centerline of the supersonic nozzle. It can be seen that the Mach number distribution within the nozzle remains relatively consistent across different inlet pressures, without significant variation due to changes in inlet pressure. The Mach number at the nozzle outlet is greater than 1, indicating that the condensation process effectively utilizes the geometric features of the supersonic nozzle, allowing for supersonic flow at the nozzle outlet. When the inlet pressure is 7.0 MPa, the outlet Mach number is 1.74, whereas at an inlet pressure of 9.0 MPa, the outlet Mach number is 1.70. The slightly higher outlet Mach number at lower inlet

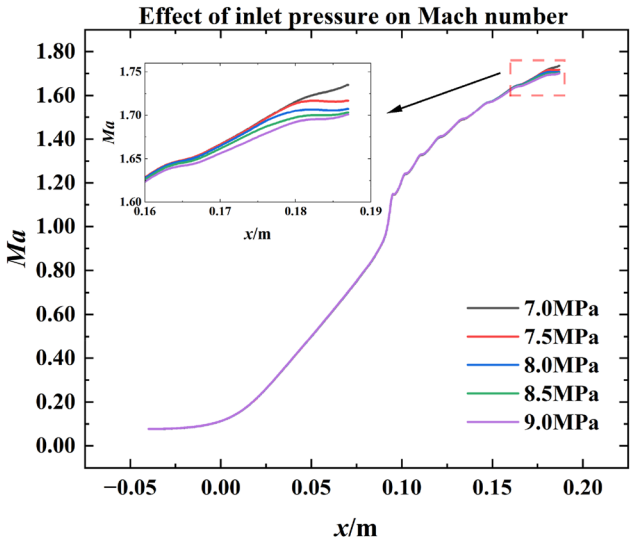

FIG. 9. Effect of inlet pressure on the centerline distribution of the Mach number within the nozzle.

pressure is due to the intensified condensation effect at higher inlet pressures, which raises the temperature at the nozzle outlet. This increase in temperature leads to a higher local speed of sound near the nozzle outlet.

Figure 5 demonstrates the influence of inlet pressure variations on the distribution of various flow parameters. For the condensation process of SCWGP in the supersonic nozzle, capturing the condensation location is also a crucial aspect. Figure 10 shows the condensation onset points at different inlet pressures, where onset of condensation corresponds to the position where the condensation rate is no longer zero. Since the condensation within a supersonic

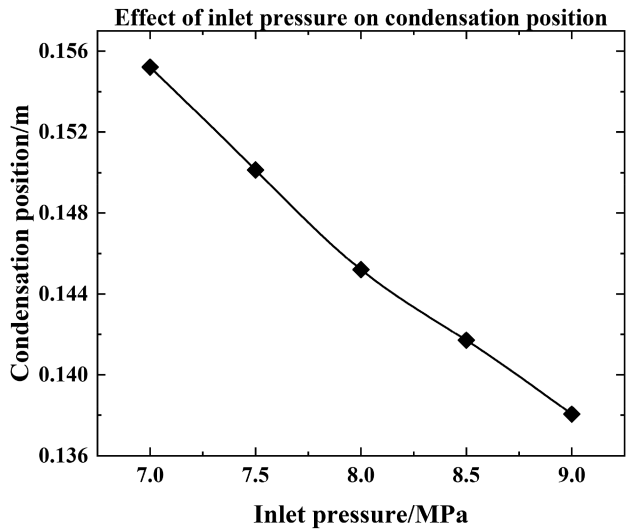

FIG. 10. Effect of inlet pressure on the condensation position on the centerline within the nozzle.

nozzle is a typical nonequilibrium process, the saturation of the SCWGP must be slightly greater than 1. This means that a certain degree of supersaturation is required for the condensation and separation process to occur. When the inlet temperature is maintained at 300.0 K, and the inlet pressure increases from 7.0 to 9.0 MPa, the condensation location shifts progressively toward the throat. It moves from 0.155 to 0.138 m, with this shift being approximately linear with respect to the change in inlet pressure.

B. Influence of inlet temperature of supersonic nozzle on condensation process

From Fig. 11, it can be observed that when the inlet pressure of the supersonic nozzle is maintained at 7.0 MPa, the pressure and temperature fields within the nozzle change as the inlet temperature gradually increases from 290.0 to 300.0 K. Additionally, the increase in inlet temperature weakens the condensation effect of the supersonic nozzle on the SCWGP, causing the condensation location to shift toward the nozzle outlet.

To derive quantitative conclusions regarding the condensation process of SCWGP within the supersonic nozzle, it is essential to further study various parameters along the nozzle centerline.

Figure 12 provides a detailed illustration of the pressure changes observed along the nozzle centerline as a result of increasing the inlet temperature from 290.0 to 300.0 K. These changes are depicted while the inlet pressure is consistently maintained at 7.0 MPa, allowing for an analysis of how temperature variations impact the pressure distribution within the nozzle under stable pressure conditions. Figure 12 shows that the pressure distribution along the centerline does not exhibit significant changes with increasing inlet temperature. However, there is a slight divergence in the pressure distribution curves at the nozzle outlet. As the inlet temperature rises from 290.0 to 300.0 K, the outlet pressure decreases from 1.30 to 1.20 MPa. Within the nozzle, condensation of SCWGP occurs, accompanied by the release of latent heat, which in turn heats the SCWGP. This release of heat not only raises the temperature of the SCWGP, but also results in a subsequent increase in pressure within the nozzle. From the pressure distribution curves in Fig. 12, it is evident that the pressure increase due to heat release from condensation is far less significant than the pressure drop due to the expansion effect within the supersonic nozzle itself. The supersonic nozzle is designed to effectively harness the pressure energy of the SCWGP in the nozzle. By doing so, it enables clean and efficient separation of the SCWGP, optimizing the overall process performance and ensuring that the separation occurs with minimal energy loss.

Figure 13 shows the impact of changes in the supersonic nozzle inlet temperature on the temperature distribution along the nozzle centerline. It can be clearly seen that owing to the anomaly caused by condensation, the outlet temperature for an inlet temperature of 290.0 K is 195.6 K, which is higher than the outlet temperature of 188.0 K for an inlet temperature of 300.0 K. This occurs because a lower nozzle inlet temperature promotes condensation within the nozzle, and the increased condensation intensifies the release of latent heat from the SCWGP. This leads to a rise in temperature within the nozzle. Additionally, Fig. 13 shows that a decrease in the nozzle inlet temperature causes the starting position of the temperature rise along the centerline to move closer to the throat of the

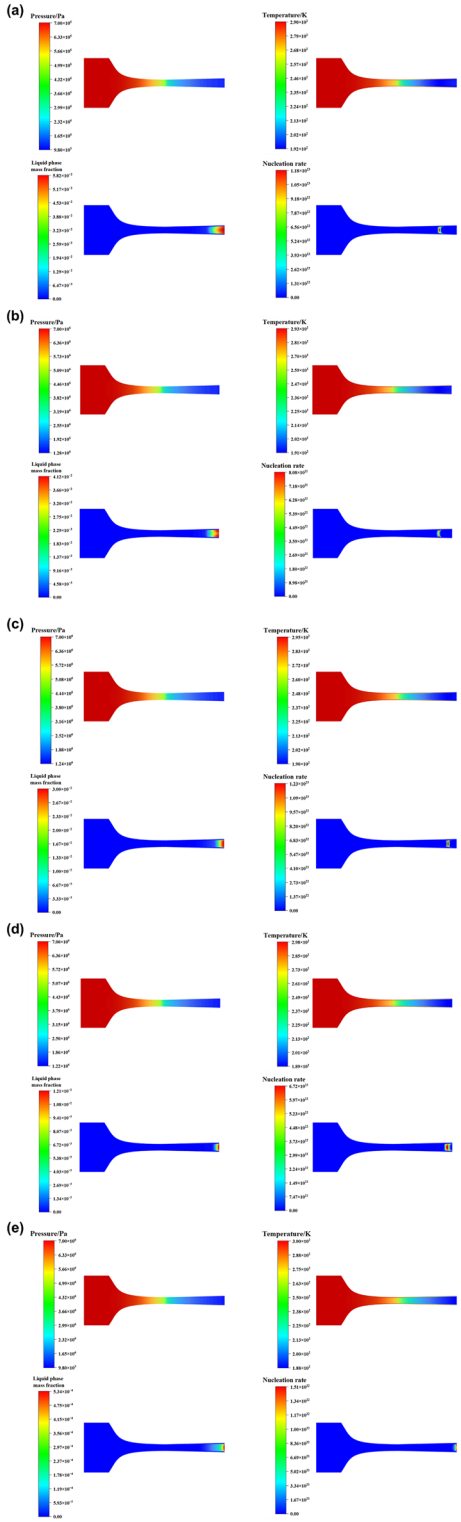

FIG. 11. Influence of the inlet temperature of a supersonic nozzle on the condensation process of SCWGP at an inlet pressure of 7.0 MPa: (a) 290.0 K; (b) 292.5 K; (c) 295.0 K; (d) 297.5 K; (e) 300.0 K.

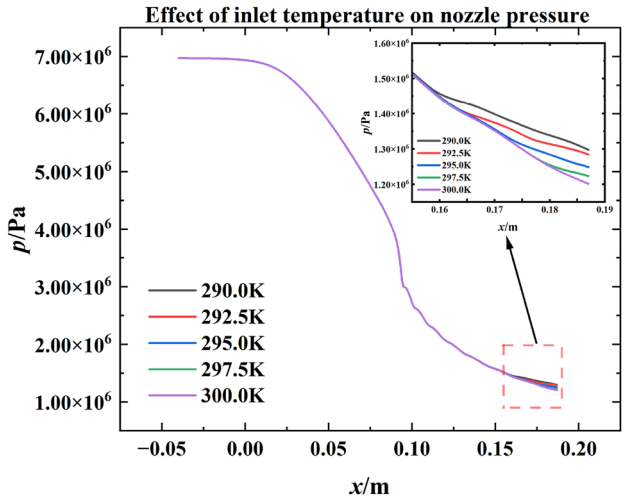

FIG. 12. Effect of inlet temperature on centerline pressure distribution within the nozzle.

nozzle. This also indicates that lowering the inlet temperature shifts the onset of condensation toward the throat.

Figure 14 shows the impact of increased inlet temperatures on the distribution of liquid phase mass fraction along the nozzle centerline during the condensation of SCWGP. As scan be seen, an increase in the inlet temperature results in a significant reduction in the liquid phase mass fraction at the nozzle outlet. Specifically, when the inlet temperature is raised from 290.0 to 300.0 K, the liquid phase mass fraction at the nozzle outlet decreases dramatically from 0.058 to 5.33×10^{-4}. Additionally, when condensation within the nozzle is intense, such as at 290.0 K, it can be observed that the

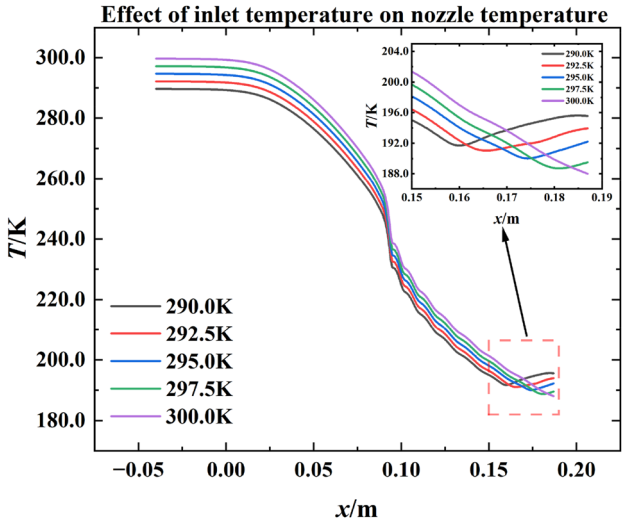

FIG. 13. Effect of inlet temperature on centerline temperature distribution within the nozzle.

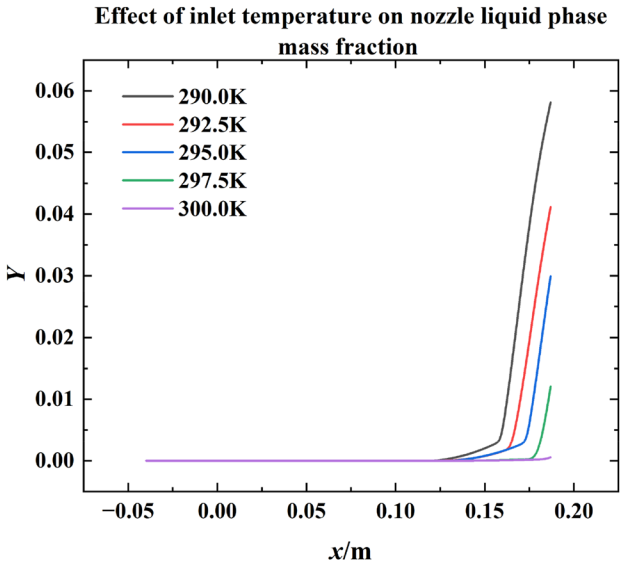

FIG. 14. Effect of inlet temperature on the centerline distribution of the liquid phase mass fraction within the nozzle.

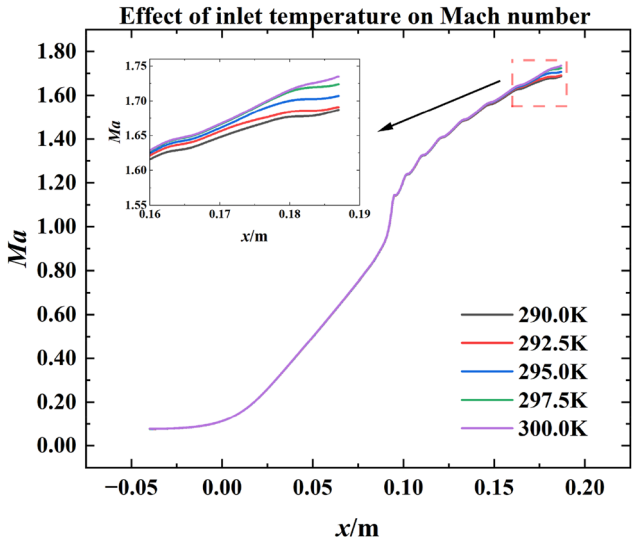

FIG. 15. Effect of inlet temperature on the centerline distribution of the Mach number within the nozzle.

liquid phase mass fraction does not increase instantly, but rather follows a two-stage growth with different rates. This suggests that the condensation rate of the SCWGP experiences a sharp peak, leading to a rapid increase in the liquid phase mass fraction. Analyzing the condensation model, we can draw the same conclusion: when the supersaturation of the SCWGP reaches a certain value, the condensation rate will rapidly increase. From the contour plots in Fig. 11, it is also clear that the condensation rate in certain regions is significantly higher than in others. And beyond these regions, owing to the decrease in saturation, intense condensation no longer occurs in the nozzle. Figure 14 also reveals that as the inlet temperature continues to rise, the starting point of the increase in liquid phase mass fraction shifts toward the outlet. This indicates that higher inlet temperatures are detrimental to full utilization of the pressure energy of SCWGP for effective condensation separation within the nozzle.

Figure 15 illustrates the impact of varying inlet temperatures on the Mach number distribution along the nozzle centerline. The data presented in this figure demonstrate that changes in the inlet temperature do not significantly affect the Mach number distribution along the centerline. This indicates that the flow characteristics within the nozzle remain relatively stable despite fluctuations in the inlet temperature. It highlights the nozzle's robustness in maintaining consistent performance under different thermal conditions. When the nozzle inlet temperature is 290.0 K, the Mach number at the nozzle outlet is 1.69, while at an inlet temperature of 300.0 K, the Mach number at the outlet is 1.74. A lower inlet temperature within the nozzle leads to intensified condensation, which in turn raises the temperature at the nozzle outlet. This increase in outlet temperature results in a higher local speed of sound at the outlet. Consequently, the Mach number at the outlet is lower when the inlet temperatures are higher, owing to the enhanced condensation effects at lower inlet temperatures. This chain of effects highlights how inlet temperature variations can influence the flow dynamics within the nozzle, particularly at the outlet.

Figure 16 illustrates the effect of inlet temperature on the condensation onset location of SCWGP within the supersonic nozzle. It can be seen that as the inlet temperature increases, the condensation onset position shifts from 0.132 m toward the nozzle outlet, reaching 0.155 m. The change in condensation position follows an approximately linear relationship with respect to the inlet temperature. Analyzing this from another perspective, it can be seen that lowering

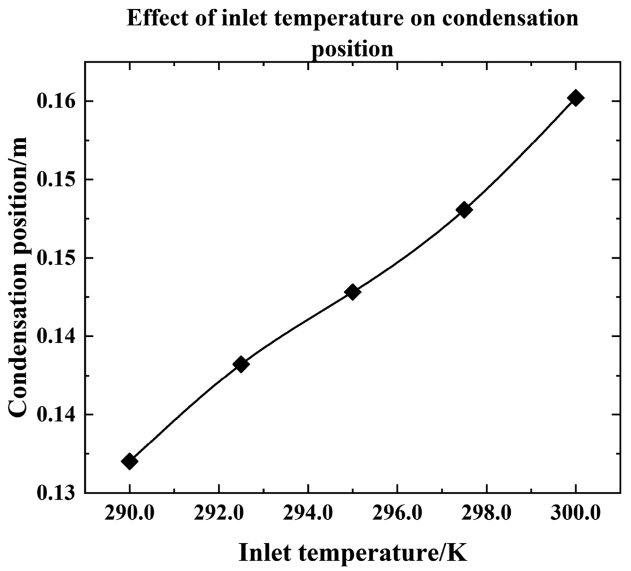

FIG. 16. Effect of inlet temperature on the condensation position on the centerline within the nozzle.

the inlet temperature of the supersonic nozzle from 300.0 to 290.0 K advances the condensation onset position by 0.023 m. According to the results in Fig. 10, an increase of 2.0 MPa in inlet pressure is required to advance the condensation position by 0.017 m when the nozzle inlet temperature remains constant. This indicates that reducing the nozzle inlet temperature is to some extent, more effective in promoting condensation within the nozzle than increasing the inlet pressure.

IV. CONCLUSION

A condensation model has been developed based on classical nucleation theory combined with a classical droplet growth model. This model has been specifically applied to modify the condensation terms in the Navier–Stokes equations governing the fluid flow. By incorporating these modifications, the model is capable of accurately capturing the flow and condensation parameters of mixed gas within a supersonic nozzle. The model allows for a more detailed understanding of the complex interactions between gas flow and condensation in such high-speed environments. The established gas flow condensation model has then been used to simulate the condensation process of the typical composition of SCWGP within a supersonic nozzle, resulting in a series of conclusions that can guide the clean and energy-efficient separation of SCWGP in industrial applications.

1. Increasing the inlet pressure of the supersonic nozzle within an appropriate range can fully leverage the nozzle's property of gas expansion cooling.
2. Condensation of SCWGP within the supersonic nozzle releases latent heat of vaporization, leading to an anomalous temperature rise in the nozzle after the condensation onset position. This temperature increase also causes a rise in pressure, but this is much smaller than the pressure drop due to the nozzle's expansion effect on the working fluid.
3. Changes in the inlet pressure and inlet temperature of the supersonic nozzle significantly impact the condensation location within the nozzle. Therefore, the condensation onset position within the nozzle can be adjusted by regulating the inlet pressure and inlet temperature of the nozzle.
4. Changes in the inlet pressure and temperature of the supersonic nozzle play a significant role in determining the liquid phase mass fraction at the nozzle outlet. Specifically, increasing the inlet pressure can lead to a higher mass fraction of condensed liquid at the outlet. Similarly, decreasing the inlet temperature can also enhance the amount of condensed liquid exiting the nozzle. These adjustments in inlet conditions directly influence the phase transition processes within the nozzle, thereby affecting the overall performance and efficiency of the separation process. The change in the liquid phase mass fraction at the nozzle outlet with changing inlet pressure is approximated to be 0.028 MPa^{-1}, and the change with changing inlet temperature is approximated to be -5.8×10^{-3} K^{-1}.
5. The condensation rate of SCWGP within the supersonic nozzle exhibits a peak, rapidly reaching its maximum value at a certain level of supersaturation before quickly declining. The peak condensation rate within the supersonic nozzle for SCWGP reaches the order of magnitude of 10^{22}–10^{23}. The region where the condensation rate is nonzero is relatively small, which leads to a rapid increase in the liquid phase mass fraction distribution.

Since the method of using a supersonic nozzle to condense and separate H_2 and CO_2 from SCWGP requires extensive simulation before actual industrial application, our future work will focus on improving the accuracy of the simulation model and finding more suitable nozzle shapes and condensation conditions. To enhance the accuracy of the simulation model, we will seek and validate newer and more reliable condensation models and strive to improve the accuracy of fluid property calculations as much as possible. Regarding the search for more suitable nozzle shapes and condensation conditions, we will base our work on realistic industrial scenarios to explore more diverse and comprehensive supersonic nozzles and condensation conditions.

AUTHOR DECLARATIONS

Conflict of Interest

The authors have no conflicts to disclose.

Author Contributions

Hongtu Wu: Conceptualization (equal); Methodology (equal); Validation (equal); Visualization (equal); Writing – original draft (equal). **Mišo Jurčević**: Supervision (equal). **Henrik Ström**: Supervision (equal). **Muhammad Shahzad Khurram**: Supervision (equal). **Hui Jin**: Conceptualization (equal); Funding acquisition (equal); Investigation (equal); Writing – review & editing (equal).

DATA AVAILABILITY

The data that support the findings of this study are available from the corresponding author upon reasonable request.

REFERENCES

[1]H. Damon Matthews, K. B. Tokarska, J. Rogelj, C. J. Smith, A. H. MacDougall, K. Haustein *et al.*, "An integrated approach to quantifying uncertainties in the remaining carbon budget," Commun. Earth Environ. **2**(1), 7 (2021).

[2]L. Das, "Near-term introduction of hydrogen engines for automotive and agricultural application," Int. J. Hydrogen Energy **27**(5), 479–487 (2002).

[3]Y. Wang, X. Zhou, and L. Liu, "Feasibility study of hydrogen jet flame ignition of ammonia fuel in marine low speed engine," Int. J. Hydrogen Energy **48**(1), 327–336 (2023).

[4]Z. Yang, M. Ghadamyari, H. Khorramdel, S. M. Seyed Alizadeh, S. Pirouzi, M. Milani *et al.*, "Robust multi-objective optimal design of islanded hybrid system with renewable and diesel sources/stationary and mobile energy storage systems," Renewable Sustainable Energy Rev. **148**, 111295 (2021).

[5]M. Mehrpooya, N. Ghadimi, M. Marefati, and S. A. Ghorbanian, "Numerical investigation of a new combined energy system includes parabolic dish solar collector, Stirling engine and thermoelectric device," Int. J. Energy Res. **45**(11), 16436–16455 (2021).

[6]P. Moriarty and D. Honnery, "When will the hydrogen economy arrive?," AIMS Energy **10**(6), 1100–1121 (2022).

[7]M. El-Adawy, M. A. Nemitallah, and A. Abdelhafez, "Towards sustainable hydrogen and ammonia internal combustion engines: Challenges and opportunities," Fuel **364**, 131090 (2024).
[8]C. Rodriguez Correa and A. Kruse, "Supercritical water gasification of biomass for hydrogen production—Review," J. Supercrit. Fluids **133**, 573–590 (2018).
[9]D. Hantoko, E. Kanchanatip, E. Kanchanatip, M. Yan, Z. Weng, Z. Gao, and Y. Zhong, "Assessment of sewage sludge gasification in supercritical water for H_2-rich syngas production," Process Saf. Environ. Prot. **131**, 63–72 (2019).
[10]S. Guo, Y. Wang, F. Shang, L. Yi, Y. Chen, B. Chen, and L. Guo, "Thermodynamic analysis of the series system for the supercritical water gasification of coal-water slurry," Energy **283**, 128646 (2023).
[11]X. Chen, Z. F. Tian, P. J. van Eyk, D. Lewis, and G. G. J. Nathan, "Numerical simulation of hydrothermal liquefaction of algae in a lab-scale coil reactor," Exp. Comput. Multiphase Flow **4**, 113–120 (2022).
[12]Y. Hu, M. Gong, X. Xing, H. Wang, Y. Zeng, and C. C. Xu, "Supercritical water gasification of biomass model compounds: A review," Renewable Sustainable Energy Rev. **118**, 109529 (2020).
[13]J. Chen, Y. Liu, X. Wu, E. Jiaqiang, E. Leng, F. Zhang, and G. Liao, "Thermodynamic, environmental analysis and comprehensive evaluation of supercritical water gasification of biomass fermentation residue," J. Cleaner Prod. **361**, 132126 (2022).
[14]Z. Chen, L. Gao, X. Zhang, W. Han, and S. Li, "High-efficiency power generation system with integrated supercritical water gasification of coal," Energy **159**, 810–816 (2018).
[15]H. R. Abid, A. Keshavarz, H. Jaffer, B. K. Nile, and S. Iglauer, "Economic material for large-scale H_2 storage and H_2-CO_2 separation," J. Energy Storage **75**, 109770 (2024).
[16]M. Shan, J. Zhang, S. Cong, Y. Zhang, X. He, F. Kapteijn, and X. Liu, "Insights into micro-structure and separation mechanism of benzimidazole-linked polymer membrane for H_2/CO_2 separation," Sep. Purif. Technol. **349**, 127732 (2024).
[17]T. Misawa, T. Ishikawa, S. Takeya, S. Alavi, and R. Ohmura, "Continuous hydrate-based CO_2 separation from H_2 + CO_2 gas mixture using cyclopentane as co-guest," J. Ind. Eng. Chem. **121**, 228–234 (2023).
[18]J. Chen, W. Jiang, C. Han, and Y. Liu, "Numerical study on the influence of supersonic nozzle structure on the swirling condensation characteristics of CO_2," J. Nat. Gas Sci. Eng. **88**, 103753 (2021).
[19]P. Yin, T. Li, X. Cao, L. Teng, Q. Li, and J. Bian, "Condensation properties of water vapor under different back pressures in nozzle," Case Stud. Therm. Eng. **31**, 101783 (2022).
[20]J. Chen, W. Jiang, C. Han, and Y. Liu, "Study on supersonic swirling condensation characteristics of CO_2 in Laval nozzle," J. Nat. Gas Sci. Eng. **84**, 103672 (2020).
[21]W. Sun, X. Cao, W. Yang, and X. Zhao, "CFD modeling on non-equilibrium condensation process of H_2S in CH_4-H_2S mixture expansion through supersonic nozzles," Fuel Process. Technol. **170**, 53–63 (2018).
[22]W. Sun, S. Chen, Y. Hou, S. Bu, Z. Ma, and L. Zhang, "Numerical studies of nitrogen spontaneous condensation flow in laval nozzles using varying droplet growth models," Int. J. Multiphase Flow **121**, 103118 (2019).
[23]J. Chen and Z. Huang, "Numerical study on carbon dioxide capture in flue gas by converging-diverging nozzle," Fuel **320**, 123889 (2022).
[24]J. Bian, X. Cao, W. Yang, X. Song, C. Xiang, and S. Gao, "Condensation characteristics of natural gas in the supersonic liquefaction process," Energy **168**, 99–110 (2019).
[25]X. Cao and J. Bian, "Supersonic separation technology for natural gas processing: A review," Chem. Eng. Process. **136**, 138–151 (2019).
[26]S. Dykas, M. Majkut, K. Smołka, and M. Strozik, "Study of the wet steam flow in the blade tip rotor linear blade cascade," Int. J. Heat Mass Transfer **120**, 9–17 (2018).
[27]S. Dykas, M. Majkut, K. Smołka, and M. Strozik, "Comprehensive investigations into thermal and flow phenomena occurring in the atmospheric air two-phase flow through nozzles," Int. J. Heat Mass Transfer **114**, 1072–1085 (2017).
[28]J. Chen and Z. Huang, "Spontaneous condensation of carbon dioxide in flue gas at supersonic state," Energy **254**, 124418 (2022).
[29]X. Wang, L. Li, and S. Wang, *Expansive Wet Steam Two-Phase Flow at High Speed* (Xi'an Jiaotong University Press, Beijing, 2018).
[30]J. Chen, Z. Huang, A. Li, R. Gao, and W. Jiang, "Carbon capture in laval nozzles with different bicubic parametric curves and translation of Witoszynski curves," Energy **260**, 125144 (2022).
[31]G. Lamanna, "On nucleation and droplet growth in condensing nozzle flows," Ph.D. thesis, Technische Universiteit Eindhoven, 2002.
[32]Y. Liu, X. Cao, J. Yang, Y. Li, and J. Bian, "Energy separation and condensation effects in pressure energy recovery process of natural gas supersonic dehydration," Energy Convers. Manage. **245**, 114557 (2021).
[33]G. Gyarmathy, "The spherical droplet in gaseous carrier streams: Review and synthesis," Multiphase Sci. Technol. **1**(1-4), 99 (1982).
[34]W. Sun, "Natural gas sweetening using supersonic swirling separation technology," Ph.D. thesis, China University of Petroleum, 2018.
[35]J. Chen, Z. Huang, and W. Jiang, "Non-equilibrium condensation of carbon dioxide in flue gas with the coexistence of swirl flows and supersonic flows," Int. Commun. Heat Mass Transfer **138**, 106369 (2022).
[36]C. Lettieri, D. Paxson, Z. Spakovszky, and P. Bryanston-Cross, "Characterization of nonequilibrium condensation of supercritical carbon dioxide in a de Laval nozzle," J. Eng. Gas Turbines Power **140**(4), 041701 (2018).
[37]J. Chen, A. Li, Z. Huang, G. Xi, and W. Jiang, "Effect of diffuser on condensing flow in nozzles for carbon capture," Fuel **342**, 127859 (2023).